Nitrogen fixation with water vapor by non-equilibrium plasma: Towards sustainable ammonia production

Yury Gorbanev, Elise Vervloessem, Anton Nikiforov, Annemie Bogaerts

Supporting Information

Pages: 19
Figures: 11
Tables: 2

Table of contents

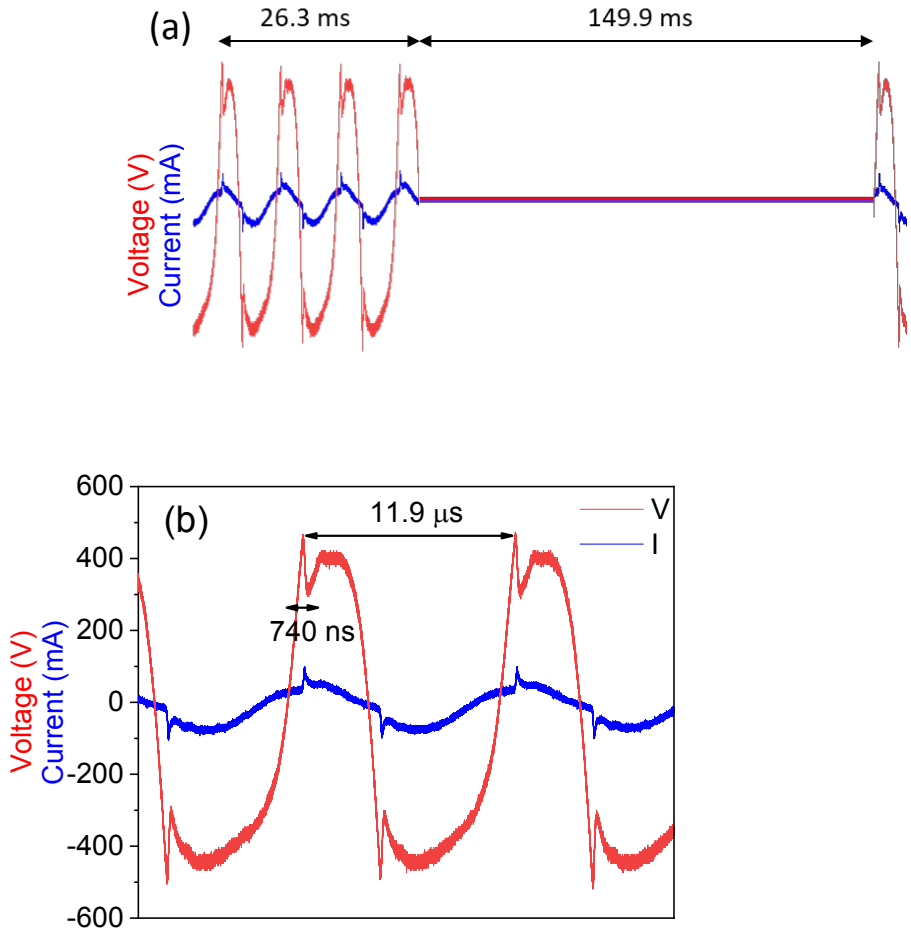

Figure S1. Voltage (V) and current (I) waveforms of the ignited plasma discharge, as measured using a voltage probe (Tektronix P6015A) and a current probe (Pearson Current Monitor 2877), connected to a LeCroy WaveSurfer 64Xs oscilloscope. (a) Schematic representation of the AC pulses (not to scale); (b) positions of the low current sparks within the AC pulses. The frequency of the AC pulses is ca. 6 Hz, and the frequency of the sparks within the AC pulses is 84 kHz. As the plasma was created only within the sparks (see below), the duty cycle of the plasma setup is 1.86%. This, together with integration of the product of V and I at the low current sparks, enables calculation of the power deposited into plasma, yielding 0.1 W.

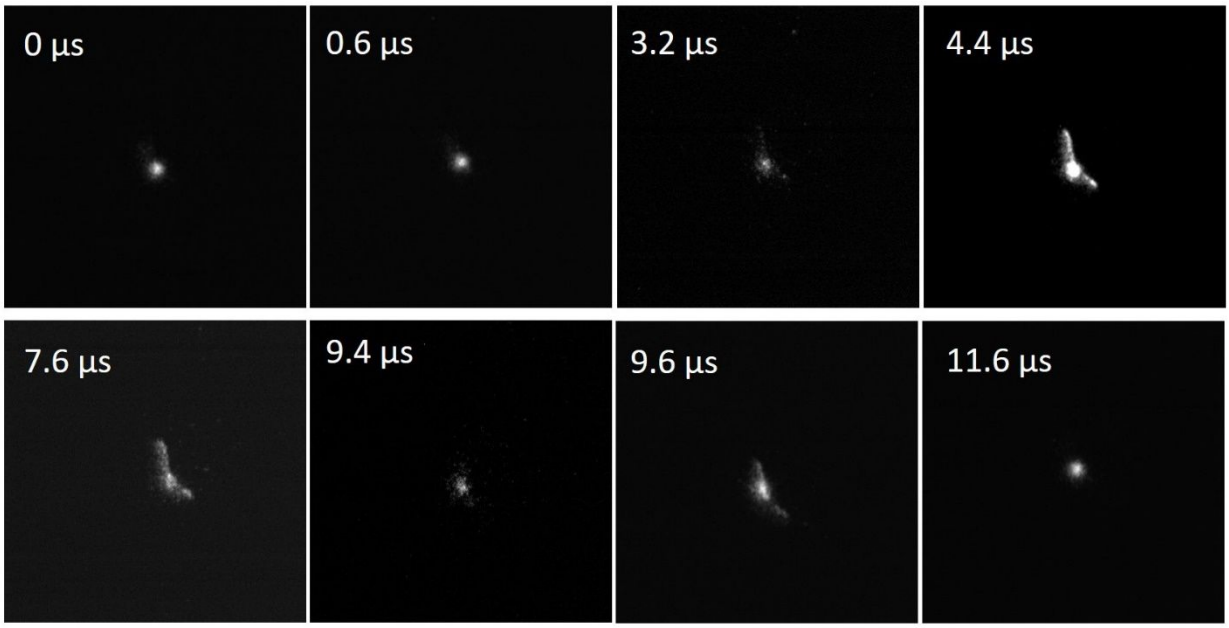

Figure S2. Time-resolved imaging of the plasma discharge obtained using a Hamamatsu C8484 ICCD camera[1] with a 100 ns exposure time. Time indication on the frames is shown in relation to the voltage crossing the zero value. The camera lens surface was perpendicular to the effluent. Plasma conditions: 0.7 L/min N_2 with 100% H_2O vapor saturation. Two low current sparks are generated at 4.4 and 9.6 µs. The intensity (i.e., brightness on the images) of the signal decreases with time, until the next spark. The visible round shape zone of low light intensity appearing in between sparks corresponds to the afterglow emission.

T1 Plasma temperature measurements

Plasma core temperature by optical emission spectroscopy (OES). In the case of non-equilibrium atmospheric pressure plasmas, the rotational temperature T_{rot} can be used as an indicator of the gas translational temperature due to the very high frequency of collisions, which leads to equilibrium between different rotational states of the colliding particles. Determination of T_{rot} assumed Boltzmann distribution of rotational/vibrational states. In this work, the OES

temperature measurements were based on relative intensity measurements of spectral lines of a second positive system of nitrogen N_2 $C^3\Pi_u \rightarrow B^3\Pi_g$ [2]. The discharge emission was collected with fibre optics (diameter 600 μm) directly facing the region where bright electrical discharge is generated. Two spectrophotometers (Avantes AvaSpec-3048, 300-390 nm) were used to partially resolve rotational structure of the N_2 bands. Spectrometers were calibrated with a 250-2400 nm halogen lamp. The rotational temperature was spatially and time averaged. MassiveOES software was used to fit the experimental and theoretical spectra, providing T_{rot} as a result of the fitting process as described in our recent work[3].

Plasma effluent by Rayleigh scattering spectroscopy (RSS). The setup for RS measurements was adapted from our recent work[4] (Figure S3). This active spectroscopic method is typically used for gas temperature measurement since the Rayleigh scattering signal (I) is proportional to the density of heavy scattered particles (n^i)[5]: $I \sim \sum_i \sigma^i n^i = \sum_i \sigma^i \frac{p}{T_g k_B}$, *w*here k_B is the Boltzmann constant and σ^i is the RS cross-section of heavy species. Gas temperature T_g is calculated as the ratio of scattered laser light intensity I_{ref} corresponding to a known reference temperature T_{ref} (room temperature during the experiments) and scattered intensity when it passes through the plasma I_p: $T_g = \frac{I_{ref}}{I_p} T_{ref}$.

The laser scattering experiments were performed in ambient conditions, with a pulsed Litron nano-S Nd:YAG laser (wavelength 532 nm, pulse energy 12 mJ, repetition rate 10 Hz, pulse duration 8 ns). The laser beam had a Gaussian shape with a diameter of 0.5 mm. The scattered light was collected, perpendicularly to the laser beam, by a Hamamatsu C8484 ICCD camera with a 532 nm filter. The synchronization between the laser pulse and the ICCD camera was achieved by the delay generator DG535.

Note that in this work, OES and RSS were complementary: RSS was used to determine the temperature of the plasma jet effluent, while the emission for OES was mostly collected from the very bright region located directly inside the plasma jet nozzle corresponding to the active discharge region.

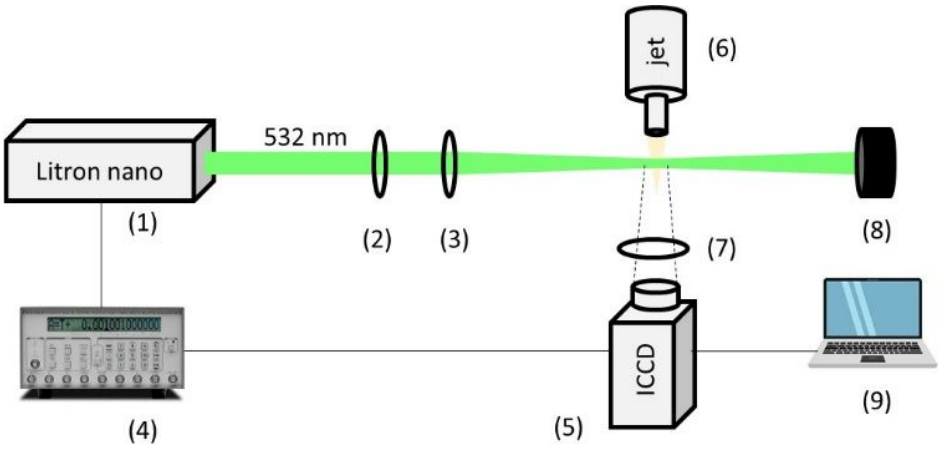

Figure S3. Rayleigh scattering spectroscopy setup including: Nd:YAG laser at 532 nm (1), polarizer (2), lens f=500 mm (3), delay generator (4), ICCD camera (5), plasma jet (6), filter 532 nm (7), beam dump (8), PC with control software (9).

Table S1. Width and average temperature of the plasma effluent with different gas flow rates at various distances from the plasma jet nozzle, as measured by Rayleigh scattering spectroscopy.

Entry	Distance from the jet (mm)	Feed gas flow rate (L/min)	H_2O vapor saturation (%)	Effluent width (mm)	Effluent temperature* (^oC)
1	1.2	0.2	-	1.2	108
2	1.2	0.35	-	1.0	91
3	1.2	0.7	-	0.9	76
4	1.2	1.4	-	0.8	47
5	1.2	0.2	100	1.1	115
6	1.2	1.4	100	0.9	57
7	3.4	0.2	-	1.8	72
8	3.4	0.35	-	1.6	75
9	3.4	0.7	-	1.3	52
10	3.4	1.4	-	1.0	35
11	3.4	0.2	100	1.8	71
12	3.4	1.4	100	1.0	38
* The average error in the temperature values obtained using Rayleigh spectroscopy was 10 ^oC.					

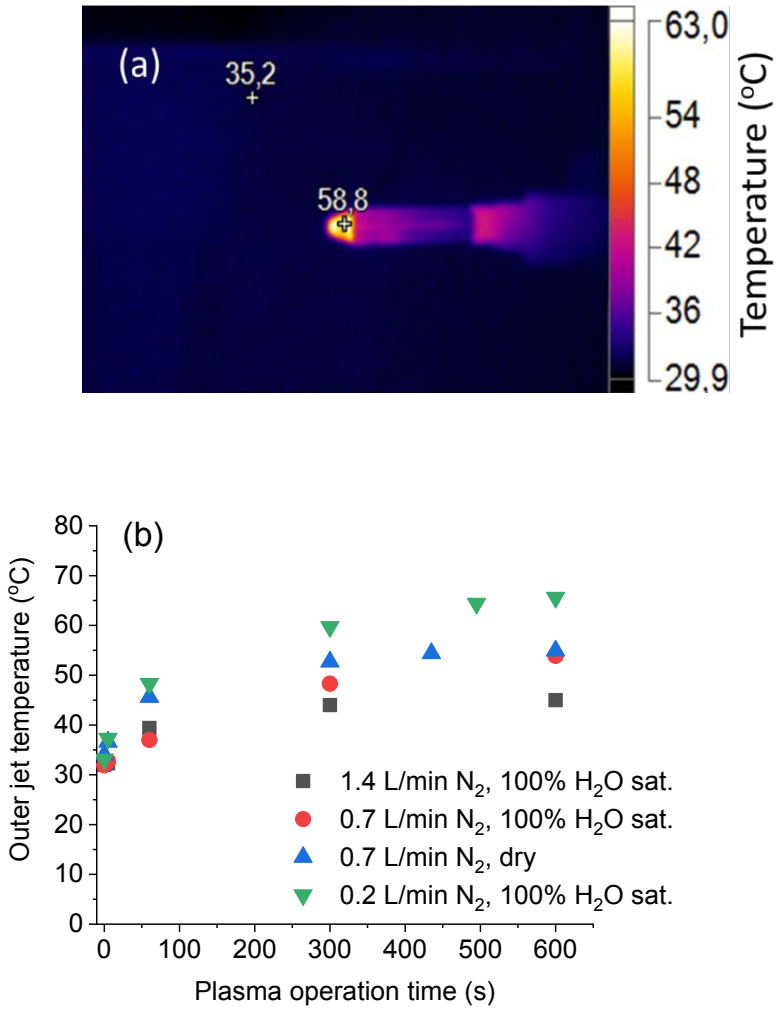

Figure S4. Temperature measurements of the outer casing of the plasma jet performed by imaging with a TiS45 Fluke IR camera. (a) A typical image obtained; (b) plasma jet outer casing temperature as a function of the plasma operation time.

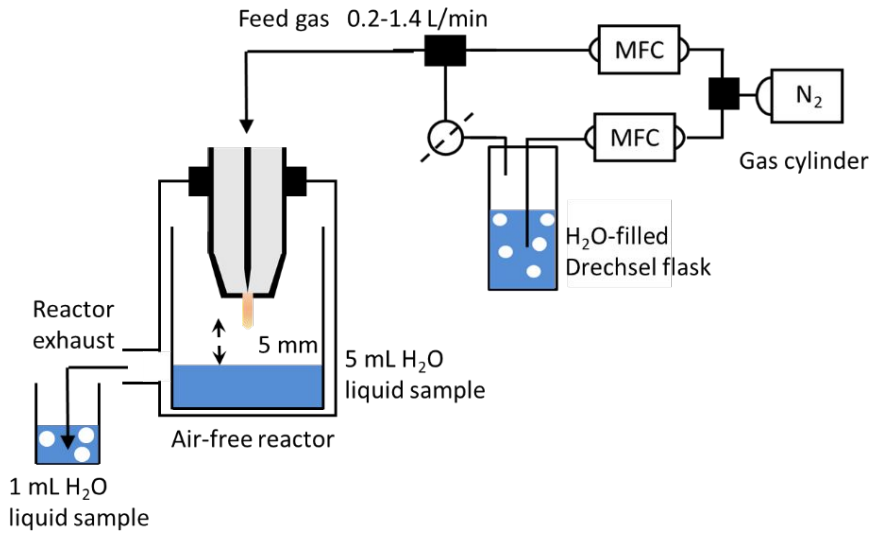

Figure S5. Experimental setup with the air-free reactor.

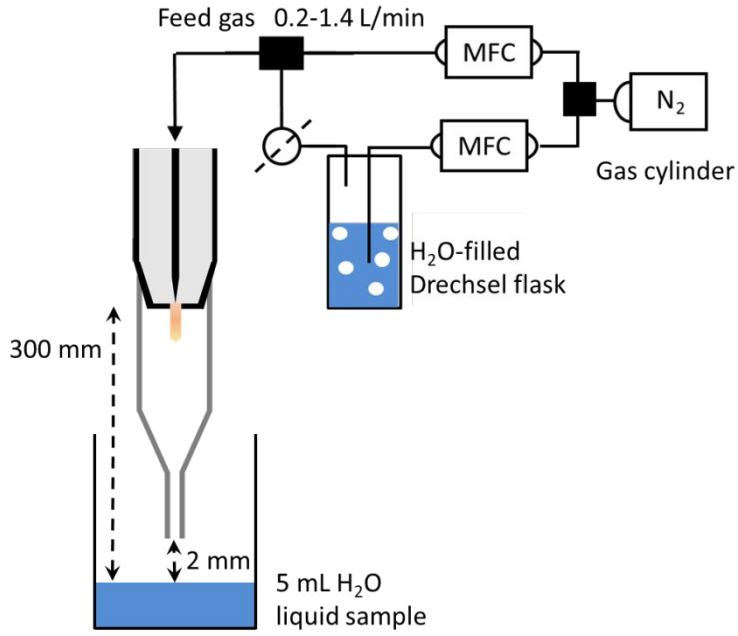

Figure S6. Experimental setup with the glass tube, eliminating the direct plasma-liquid interaction.

T2 Materials

$K_2TiO(C_2O_4)_2•2H_2O$ (≥98%), H_2SO_4 (97%), NaN_3 (≥98%), H_2O_2 (30 wt%) used for H_2O_2 measurements, and HCl (37%), CH_3COOH (100%), $NH_4Fe(SO_4)_2•12H_2O$, 1,10-phenanthroline (≥99%), NH_2OH (50 wt%) for NH_2OH measurements, were purchased from Sigma.

Spectroquant Hydrazine Test Kit and $NH_2NH_2•H_2O$ (≥99%) for NH_2NH_2 analysis were obtained from VWR.

The Nitrate/Nitrite Colorimetric Assay Kit and LabAssay Ammonia Kit were purchased from Cayman Chemicals and Fujifilm Wako Pure Chemical Corporation, respectively.

D_2O (99.9%) was from Sigma Aldrich. N_2 (99.999%) and compressed air were supplied by Praxair.

De-ionized H_2O was used to prepare all solutions.

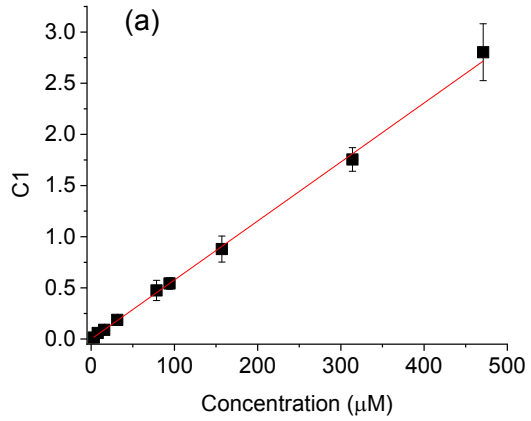

Equation	y = a + b*x
Plot	Absorbance
Weight	Instrumental
Intercept	0 B± --
Slope	0.00577 B± 1.18
Residual Sum of S	1.95686
Pearson's r	0.99832
R-Square(COD)	0.99665
Adj. R-Square	0.99623

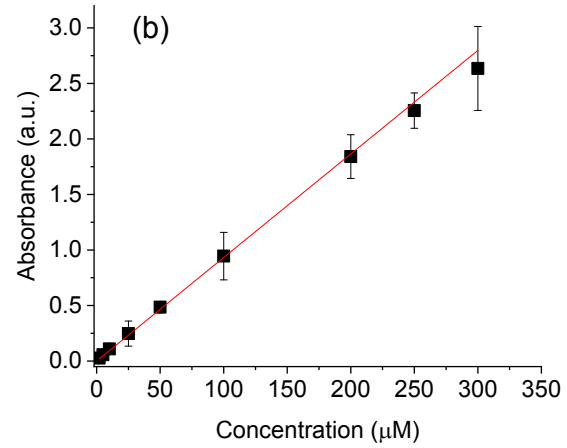

Equation	y = a + b*x
Plot	C1
Weight	Instrumental
Intercept	0
Slope	0.00933
Residual Sum of Sq	2.35884
Pearson's r	0.99766
R-Square(COD)	0.99533
Adj. R-Square	0.99475

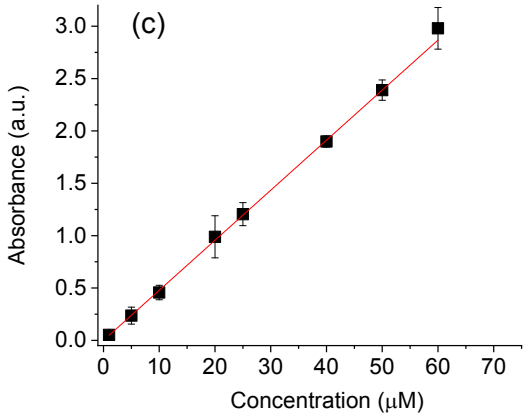

Equation	y = a + b*x
Plot	Absorbance at 46
Weight	Instrumental
Intercept	0
Slope	0.04779
Residual Sum of Sq	0.5845
Pearson's r	0.99987
R-Square(COD)	0.99975
Adj. R-Square	0.99971

Figure S7. Calibration curves for the measurement of (a) NH_3, (b) NH_2OH and (c) NH_2NH_2 in liquid H_2O samples.

T3 Measurements of NH_3, NH_2OH and NH_2NH_2 concentrations in the plasma-exposed water by colorimetry

The measurements were performed on a UV-Vis Thermo Fischer Genesys 6 spectrophotometer using Hellma quartz cuvettes with a 10 mm path length.

NH_3 measurement procedure: 140 μL of Chromogen A (from the LabAssay Ammonium kit) were mixed with 140 μL of the NH_3-containing H_2O solution; after 30 min of incubation, 70 μL of Chromogen B were added; after another 30 min of incubation, 140 μL of Chromogen C were added, and the resulting mixture was incubated for 2 h. The absorbance was measured at the peak maximum of 637 nm.

NH_2OH measurement procedure: 1.2 mL of the NH_2OH-containing solution was mixed with 100 μL of a 5:6 mixture of 1 M CH_3COONa and 1 M CH_3COOH. Then, 100 μL of 4 mM $NH_4Fe(SO_4)_2$•$12H_2O$ in 0.1 M HCl were added. After the solution was vigorously stirred for 2 min, 100 μL of 1,10-phenanthroline in 0.1 M HCl were added, and the resulting mixture was incubated for 30 min. The absorbance was measured at the peak maximum of 510 nm.

NH_2NH_2 measurement procedure: 1 mL of the NH_2NH_2-containing solution was mixed with 100 100 μL of the Hy-1 reagent from the Spectroquant Hydrazine Test Kit, and incubated for 10 min. The absorbance was measured at the peak maximum of 458 nm.

T4 Selectivity of NH_3, NH_2OH and NH_2NH_2 colorimetric measurements in the plasma-exposed water

We performed extensive tests to determine the influence of possible other N_2 fixation and plasma-H_2O interaction products on the selectivity of the UV-Vis spectrophotometric analysis used. We cross-tested each of the species: NH_3, NH_2OH, and NH_2NH_2, together with NO_2^-, NO_3^-

, and H_2O_2 (i.e., all possible long-lived species in the plasma-exposed H_2O). NO_2^- was added as $NaNO_2$ (98%), and NO_3^- as KNO_3 (99%), obtained from Alfa Aesar.

NH_3 analysis selectivity with the LabAssay Ammonium kit. The calibration curve of NH_3 in absence of any other species is shown in Figure S7a. Of all tested species, only NH_2OH and NH_2NH_2 exhibited a potential to directly interfere with the colorimetric analysis: they both produced an absorbance peak with a maximum at 637 nm. NH_2OH gave much stronger interference than NH_2NH_2. Here, 1 mM concentration of commercial NH_2NH_2 gave an absorption signal of ca. 0.040 a.u. This would correspond to 7 μM of NH_3 (Figure S7a). Therefore, unless NH_2NH_2 is produced in very large quantities, its interference can be disregarded. At the same time, NH_2OH gave much stronger absorption values, as shown in Figure S8. Therefore, NH_2OH concentrations must be measured, and included in the calculation of NH_3 concentrations. However, we note that in our experiments we did not observe any NH_2NH_2 or NH_2OH in H_2O after the plasma exposure (see below).

The overall analysis is based on the modified method developed by Ito et al.[6] NH_3 is converted to dioxydiphenylamine (DODPA) via the reaction with phenol and $Na[Fe(CN)_5NO]$. DODPA is further oxidized to indophenol blue by ClO^-. H_2O_2 and NO_2^- in the plasma-exposed H_2O could react with ClO^- [7] which is added as one of the Chromogens in the kit. However, ClO^- is added in a large excess, making the chosen method suitable for our experiments.

NH_2OH analysis selectivity. The only interference was from H_2O_2. However, the absorbance signal at 510 created in the analysis method by 1 mM H_2O_2 was ca. 0.051 a.u., corresponding to 5.5 μM NH_2OH (Figure S7b). In all our experiments, the concentration of H_2O_2 did not exceed ca. 50 μM (see Figure 2 in the main text). In any case, we did not detect any absorbance peaks at 510 nm when analysing the plasma-exposed H_2O solutions. However, NH_2OH can react with

NO_2^- [8]. Thus, although we cannot exclude that some NH_2OH can be produced in situ during the plasma exposure, it is lost in a reaction with NO_2^-.

We explicitly note that the selectivity reported in our work is based on the final concentrations of the N_2 fixation products in H_2O, after the plasma exposure.

NH_2NH_2 analysis selectivity with the Spectroquant Hydrazine Test Kit. We did not observe any detectable analysis interferences for NH_2NH_2. Futhermore, in analysis of all experiments we did not observe the induction of an absorbance peak at 458 nm, i.e., no NH_2NH_2 was detected.

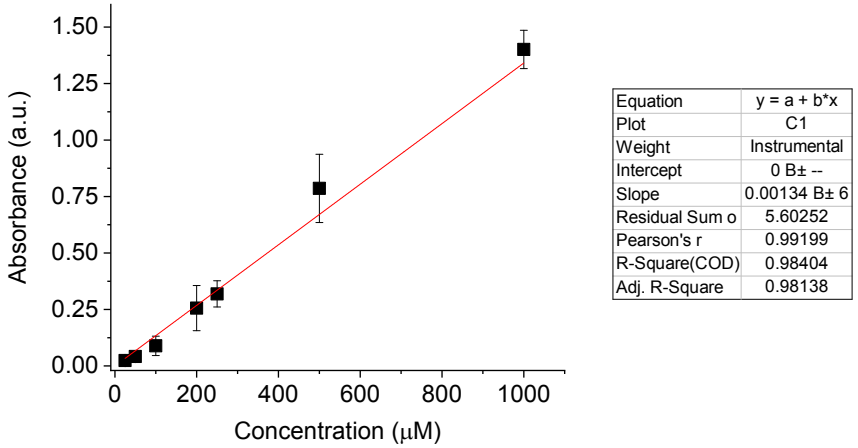

Figure S8. Absorption signal at 637 nm produced by various concentrations of NH_2OH using the LabAssay Ammonium Kit.

T5 Energy consumption calculation

The power deposited in the plasma (DP) was 0.1 W (see Figures S1 and S2 above). The conditions which allow highest NH_3 selectivity were 0.2 L/min N_2, with 5-10% H_2O vapor saturation. Under these conditions, the production rate (PR) of NH_3 was 0.052-0.064 mg/h (Table S2). The energy consumption (EC) is calculated as $\mathrm{EC\ (J/mol)} = \frac{\mathrm{DP\ (W)}}{\mathrm{PR\ (mg/h)}} \times 3600 \left(\frac{\mathrm{s}}{\mathrm{h}}\right) \times 17000 \left(\frac{\mathrm{mg}}{\mathrm{mol}}\right)$. Under the conditions mentioned above, EC was 95-118 MJ/mol NH_3.

Table S2. Rate and selectivity of NH_3 production, and conversion of N_2, by the plasma jet as a function of H_2O vapor content at different gas flow rates.

Entry	Feed gas flow rate (L/min)	H_2O vapor saturation (%)	NH_3 production rate (mg/h)	NH_3 selectivity (%)*	N_2 conversion (%)**
1		-	0.031	88	0.0004
2		2	0.044	95	0.0006
3		5	0.052	96	0.0007
4	0.2	10	0.064	95	0.0008
5		20	0.078	86	0.0011
6		50	0.107	65	0.0020
7		100	0.124	63	0.0023
8		-	0.031	86	0.0002
9		2	0.037	93	0.0003
10		5	0.053	94	0.0004
11	0.35	10	0.063	93	0.0005
12		20	0.077	81	0.0007
13		50	0.135	68	0.0014
14		100	0.153	65	0.0016
15		-	0.032	78	0.0001
16		2	0.036	88	0.0001
17		5	0.058	91	0.0002
18	0.7	10	0.072	89	0.0003
19		20	0.074	87	0.0003
20		50	0.169	65	0.0009
21		100	0.184	63	0.0010
22		-	0.029	73	0.0001
23		2	0.038	86	0.0001
24		5	0.064	88	0.0001
25	1.4	10	0.072	84	0.0001
26		20	0.096	83	0.0002
27		50	0.216	66	0.0006
28		100	0.263	64	0.0007

*Calculated as $\frac{\mathrm{C(NH3)\ mol/L}}{\mathrm{C(NH3 + NO2-\ + NO3-)\ mol/L}} \times 100\ \%$.

**Calculated as $\frac{\mathrm{C(NH3 + NO2-\ + NO3-)\ mol/L}}{10\ \mathrm{min}} \times \frac{5\ \mathrm{mL}}{1000\ \mathrm{mL/L}} \times 24.5\ \mathrm{L/mol} \times \frac{1}{\mathrm{FR\ L/min}} \times 100\%$, where FR is the flow rate of the gas. This is based on the assumption that all N_2 fixation products are converted into NH_3, NO_2^-, or NO_3^-.

T6 Calculation of ΔG values

The values of ΔG for the reaction $2N_2 + 6H_2O \rightarrow 3O_2 + 4NH_3$ were calculated as shown below using the data from literature[9]. The calculation was based on the following assumptions: 1) the reactions occur in the gas phase, with all reactants and products in the gaseous state; 2) C_p is constant within the used temperature range; 3) partial pressures of the products were estimated from the stoichiometry of the reaction and the conversion values of N_2 (see Table S2). The values of ΔG were calculated for two 'envelope' conditions: 298 K, and the highest measured temperature in our plasma system (1623 K). The ΔG values at all other possible temperature values belong to this range.

At 298 K, $\Delta G^0 = \Delta G_f^0 (NH_3)\times 4 - \Delta G_f^0 (H_2O)\times 6 + RTlnK$ = ca. 1.2 MJ/mol, where $K = P_{O2}^3 \times P_{NH3}^4 / (P_{H2O}^6 \times P_{N2}^2)$. At other temperatures, ΔH_f and S values of each compound were calculated as $\Delta H_f^0 + C_p\Delta T$, and $S^0 + C_p ln(T/298)$, respectively. ΔG was calculated as $\Delta H_f - T\times\Delta S + RTlnK$. At 1623 K, ΔG is 0.9 MJ/mol.

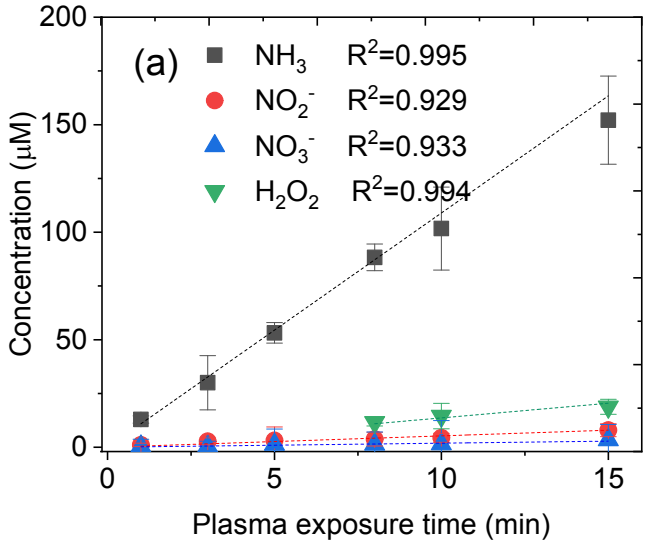

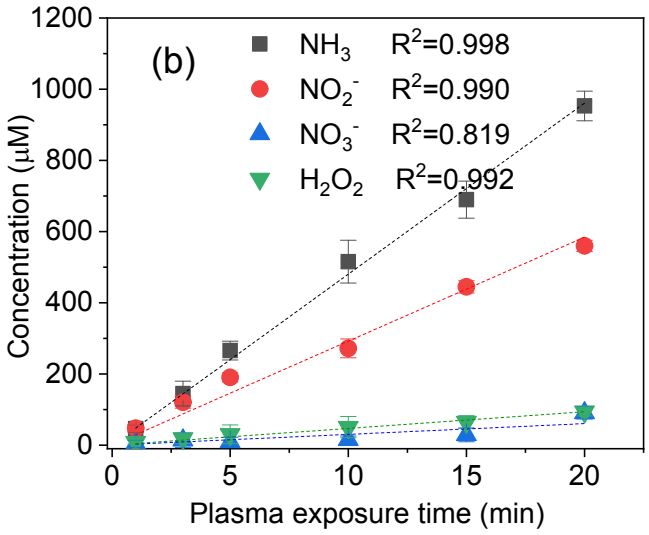

Figure S9. Concentration of the produced NH_3, NO_2^-, NO_3^-, and H_2O_2 in liquid H_2O as a function of plasma exposure time. Plasma conditions: (a) 0.2 L/min N_2, 5% H_2O vapor saturation; (b) 1.4 L/min N_2, 100% H_2O vapor saturation. Liquid volume 5 mL, distance from plasma jet to liquid 5 mm. R^2 values are given for linear $y=kx$ fittings.

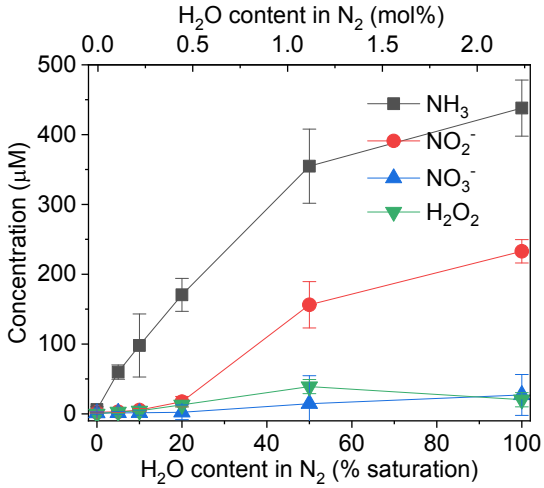

Figure S10. Concentration of the produced NH_3, NO_3^-, NO_2^-, and H_2O_2 in liquid H_2O with 1.4 L/min N_2, as a function of H_2O vapor saturation. Liquid volume 5 mL, distance from plasma jet to liquid 300 mm, exposure time 10 min. This Figure corresponds to Figure 5 (main text), but at a higher flow rate.

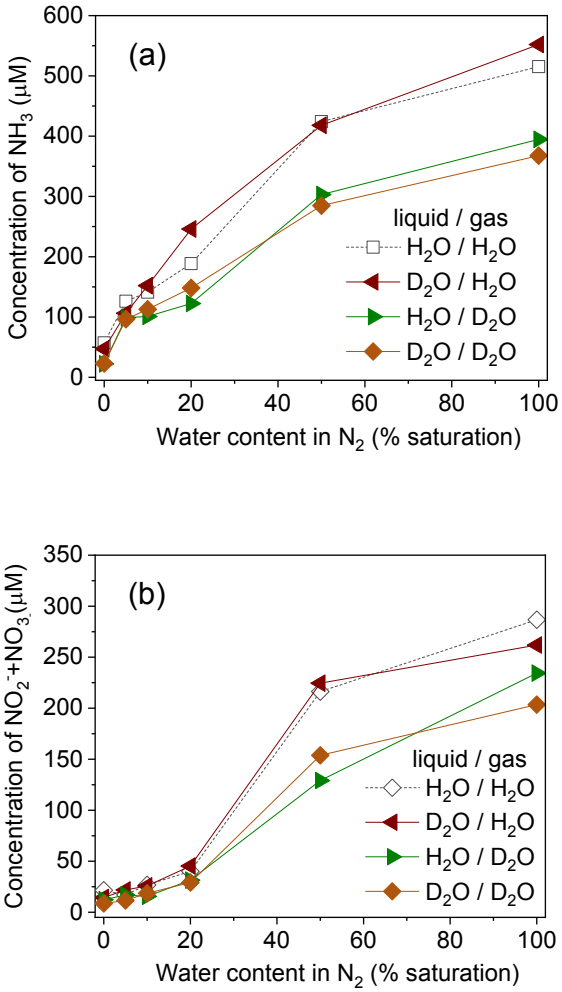

Figure S11. Concentration of NH_3, NO_3^-, NO_2^-, as a function of water vapor saturation, with 1.4 L/min N_2 flow rate. (a) NH_3 concentration; (b) total NO_2^-+NO_3^- concentration. Liquid volume 5 mL, distance from plasma jet to liquid 5 mm, exposure time 10 min. Experimental data with H_2O liquid and H_2O vapor were added here as dashed lines for comparison. This Figure corresponds to Figure 6 (main text), but at a higher flow rate.

REFERENCES

1. Xiong, Q.; Nikiforov, A. Y.; Lu, X. P.; Leys, C., High-speed dispersed photographing of an open-air argon plasma plume by a grating–ICCD camera system. *J. Phys. D: Appl. Phys.* **2010,** *43* (41), 415201-415210. DOI: 10.1088/0022-3727/43/41/415201.

2. Herzberg, G., *Spectra of Diatomic Molecules*. Krieger Publishing Company: Malabar, Florida, USA, 1989.

3. Sremački, I.; Gromov, M.; Leys, C.; Morent, R.; Snyders, R.; Nikiforov, A., An atmospheric pressure non-self-sustained glow discharge in between metal/metal and metal/liquid electrodes. *Plasma Process. Polym.* **2019**, DOI: 10.1002/ppap.201900191.

4. Barletta, F.; Leys, C.; Colombo, V.; Gherardi, M.; Britun, N.; Snyders, R.; Nikiforov, A., Insights in plasma-assisted polymerization at atmospheric pressure by spectroscopic diagnostics. *Plasma Process. Polym.* **2019**, DOI: 10.1002/ppap.201900174.

5. Miles, R. B.; Lempert, W. R.; Forkey, J. N., Laser Rayleigh scattering. *Meas. Sci. Technol.* **2001,** *12* (5), R33-R51. DOI: 10.1088/0957-0233/12/5/201.

6. Ito, S.; Takaoka, T.; Kishi, S.; Okuda, H.; Fujii, S., Studies of the clinical application of serum leucine aminopeptidase (LAP) activity determined with leucinamide as substrate. *Gastroenter. Jpn.* **1975,** *10* (1), 20-28. DOI: 10.1007/bf02775920.

7. Jirásek, V.; Lukeš, P., Formation of reactive chlorine species in saline solution treated by non-equilibrium atmospheric pressure He/O2 plasma jet. *Plasma Sources Sci. Technol.* **2019,** *28* (3), 035015-035038. DOI: 10.1088/1361-6595/ab0930.

8. Bothner-By, A.; Friedman, L., The Reaction of Nitrous Acid with Hydroxylamine. *J. Chem. Phys.* **1952,** *20* (3), 459-462. DOI: 10.1063/1.1700442.

9. Wagman, D. D.; Evans, W. H.; Parker, V. B.; Schumm, R. H.; Halow, I.; Bailey, S. M.; Churney, K. L.; Nuttall, R. L., The NBS tables of chemical thermodynamic properties. *J. Phys. Chem. Ref. Data* **1982,** *11*, suppl. 2.